Journal of Nuclear Materials 389 (2009) 93–97

Contents lists available at ScienceDirect

Journal of Nuclear Materials

journal homepage: www.elsevier.com/locate/jnucmat

Phase relations in the U–Mo–Al ternary system

H. Noël [a,*], O. Tougait [a], S. Dubois [b]

[a] Laboratoire de Chimie du Solide et Matériaux, UMR6226, CNRS, Université de Rennes1, Avenue du Général Leclerc, 35042 Rennes, France
[b] CEA, Cadarache, DEN/DEC/SPUA, 13108 St Paul lez Durance, France

A B S T R A C T

The phase relations in the U–Mo–Al system of quenched samples annealed at 800 °C for 2 weeks and at 400 °C for 2 months have been established using X-ray powder diffraction, scanning electron microscopy and energy dispersive spectroscopic analysis performed at room temperature. Two ternary Al-rich phases, $UMo_{2-x}Al_{20+x}$ and $U_6Mo_{4+x}Al_{43-x}$ are found stable at 800 °C and 400 °C. They show significant homogeneity ranges resulting from Mo/Al substitution mechanism on various mixed crystallographic sites, as evidenced by single-crystal structure refinements. Substitution of up to 25 at.% of Al by Mo atoms is also observed for UAl_2 (cubic $MgCu_2$-type) giving a quite large extension ($UAl_{2-x}Mo_x$, $0 < x < 0.5$) into the ternary system. Larger substitution ($0.6 < x < 0.7$ at $T = 800$ °C) stabilizes another ternary Laves phase, $UAl_{2-x}Mo_x$ with the hexagonal $MgZn_2$-type. There is no detectable solubility of Mo in UAl_4, and it is of the order of 1 at.% in UAl_3. The interaction layers between the γU–Mo alloys and the Al matrix in nuclear fuel plates can be successively estimated as composed of the two- and three-phase fields equilibrium indicated on the assessment of the phase relations drawn for samples heat-treated at 400 °C.

1. Introduction

The cubic bcc γ-form of uranium metal may be easily stabilised down to room temperature by alloying with other metals such as molybdenum with a content of 6 wt% or higher [1]. Based on its high stability under irradiation, a high density γ-U–Mo alloy (with 7–10 wt% Mo, denoted U–7Mo or U–10Mo) has been considered to be the best candidate as a low enriched (LEU), non-proliferant, uranium fuel for research and test reactors. However, an interaction occurs between the U–Mo alloy and the surrounded aluminium, used for fuel heat evacuation.

In-pile experiments have thus shown that dispersed U–Mo fuel in a pure Al matrix does not withstand high operating conditions [2–4]. Extensive porosity is formed in the interaction layer, at the fuel/matrix interface, resulting in an unacceptable pillowing and/or swelling of the fuel plate. The behaviour of this interaction seems to be responsible, directly or indirectly, for such a limit. Out-of-pile experiments have shown similar phenomena: U–Mo/Al interaction [5,6] and, at times, a large amount of porosities [7]. The out-of-pile mechanisms, which are probably different from the in-pile ones, have to be considered in order to understand the U–Mo/Al system and then select solutions to prevent (or at least limit) this fuel/matrix interaction.

In order to gain further knowledge on the U–Mo fuel behaviour, and to propose solutions to its operating limit, a full knowledge of the phase relations in the U–Mo–Al ternary system is essential.

Up to now, phase relations in the U–Mo–Al ternary system have not been fully determined. Previous investigations were limited to the partial isothermal sections at 500 °C, 1050 °C and 1250 °C for the composition range U–Mo–Mo_3Al_8–UAl_2 [8]. This composition domain is the Al-poor part of the system, which does not give much information on the direct interaction at the interface U–Mo/Al. The main reported feature is the formation of a rather extended homogeneous region $UAl_{2-x}Mo_x$ with a cubic structure, corresponding to the substitution of Al by Mo in the binary aluminide UAl_2, up to $x = 0.66$. It changes into a hexagonal phase at the higher substitution ratio. Two ternary compounds were subsequently discovered in the Al-rich part of the system: UMo_2Al_{20} which crystallizes in the cubic structure type $CeCr_2Al_{20}$ (space group $Fd\bar{3}m$) [9], and $U_6Mo_4Al_{43}$ which crystallizes with the hexagonal $Ho_6Mo_4Al_{43}$ structure type (space group $P6_3/mcm$) [10]. In order to obtain a complete information on phase formation and phase relations, we have assessed at room temperature the ternary sections of the U–Mo–Al phase diagram on air-quenched sample heat-treated at 400 °C and 800 °C, respectively, close to the temperature of hot rolling manufacturing process and close to the in-pile incidental temperature.

2. Experimental

For each of the two annealing temperatures, about forty samples were prepared, covering the entire ternary composition domain. High purity metals, uranium pieces (99.8 wt%), molybdenum chips (99.99 wt%) and aluminium rods (99.999 wt%) were arc-melted in a water-cooled copper-hearth under an atmosphere of purified argon.

* Corresponding author. Tel.: +33 223236255; fax: +33 223236799.
E-mail address: henri.noel@univ-rennes1.fr (H. Noël).

0022-3115/$ - see front matter © 2009 Elsevier B.V. All rights reserved.
doi:10.1016/j.jnucmat.2009.01.013

The buttons were melted three times (weight losses <1%) to ensure a proper homogeneity. A part of each as-cast alloys were annealed in silica tube sealed under residual atmosphere of argon, either at 400 °C or 800 °C for 1–2 months and for 2 weeks–1 month, respectively. After the heat-treatment, the samples were quenched in air. Samples taken from both as-cast and heat-treated buttons were ground into powder for X-ray powder diffraction experiments and embedded into resin before being polished down to 1 μm for optical microscopic observations, scanning electron microscopy coupled with energy dispersive spectroscopy (SEM–EDS) analyses.

Single-crystal X-ray diffraction data were collected on a Nonius Kappa CCD diffractometer, using well-established procedures [11].

Differential thermal analysis (DTA) was performed on some samples using a Setaram Labsys device operating up to 1600 °C.

3. Results and discussion

3.1. The U–Mo–Al phase diagram of quenched samples heat-treated at 800 °C

The phase relations in U–Mo–Al ternary alloys annealed at 800 °C are shown in Fig. 1.

3.1.1. The binary and pseudo-binary systems

3.1.1. a. Literature data. According to literature (Massalski [12]) the following binary phases are stable at 800 °C: UAl_2 (Cubic, $Pm\bar{3}m$), UAl_3 (cubic, $Pm\bar{3}m$), Mo_3Al (cubic, $Pm\bar{3}n$), Mo_3Al_8 (monoclinic, C2/m), and Mo_4Al_{17} (monoclinic, C2). The later composition is indicated in a more recent compilation of binary intermetallic systems (Pauling File [13]), following a partial re-investigation of the Mo–Al system [14] which also notifies the existence of another phase with very close composition: Mo_5Al_{22}, but which is stable only in a narrow temperature range (831–964 °C). Uranium in the cubic (γ) form constitutes a solid solution with Mo up to 40 at.%(Mo), and dissolves about. 3 at.% Al. The solubility of Al in Mo is shown to be about 2 at.%, at 800 °C. According to the Mo–U equilibrium phase diagram published in Massalski [12], the cubic U–Mo alloys are not stable at room temperature, and should transform into a two-phases mixture of the binary U_2Mo and orthorhombic αU dissolving about 1% Mo.

3.1.1. b. Experimental data. The formation and stability at 800 °C of the reported U–Al and Mo–Al binary phases have been confirmed. The solubility of Al in Mo is found to extend up to 12 at.% Al. The mutual solubility of Mo and Al in U extends up to 38 at.%Mo and 3%Al, forming a ternary field, where the cubic U(γ) form is easily retained after quenching to room temperature in alloys containing more than ≈10 at.% Mo, the transformation to the orthorhombic α form occurring for lower Mo contents. These results are in full agreement with previous studies on quenched U–Mo alloys [1,15,16], but are in conflict with the assessed binary Mo–U equilibrium phase diagram. The quenched γU–Mo alloys adopting the cubic γ form are then expected to be in a metastable state at room temperature. However, although this Mo–U binary phase diagram is generally accepted as a reference, the associated comments [12] stipulate that *'the Mo–U phase diagram certainly needs revision'*.

The substitution of Al by Mo atoms in the cubic ($MgCu_2$ type) binary UAl_2 leads to an extended solid solution $UAl_{2-x}Mo_x$ up to $x = 0.5$, but such substitution in UAl_3 is nearly negligible, being of the order of 1 at.% (precision limit of the elementary EDS analysis).

Consequently, the substitution of Mo atoms to Al sites in the ternary extension of binary phases leads to $U(Al_{2-x}Mo_x)$-type notation, rather than $(U,Mo)Al_x$ commonly written in previous papers [17], but which is misleading concerning atomic site occupation.

3.1.2. Ternary compounds and phase relations

A Laves phase with the hexagonal $MgZn_2$ type is formed within the composition range $UAl_{2-x}Mo_x$ with $0.6 \leqslant x \leqslant 0.7$. A striking feature is that the previously mentioned ternary extension of the binary UAl_2, with the $MgCu_2$ type, forms a two-phase field with the α form of the U–Mo alloy, while the γ form of the U–Mo alloy, which is of interest as nuclear fuel, is in equilibrium with the hexagonal $MgZn_2$-type.

The formation of the other previously known ternary compounds UMo_2Al_{20} and $U_6Mo_4Al_{43}$ [9,10] was also confirmed. However, the synthesis of ternary alloys with the stoichiometric composition 6:4:43 systematically led to three-phase mixtures. Fig. 2 shows the typical microstructure of a sample $U_6Mo_4Al_{43}$ annealed at 800 °C during 2 weeks (no further changes being observed for longer time annealing), showing the three-phase equilibrium UAl_3–$U_6Mo_4Al_{43}$–UMo_2Al_{20}. In fact, X-ray powder

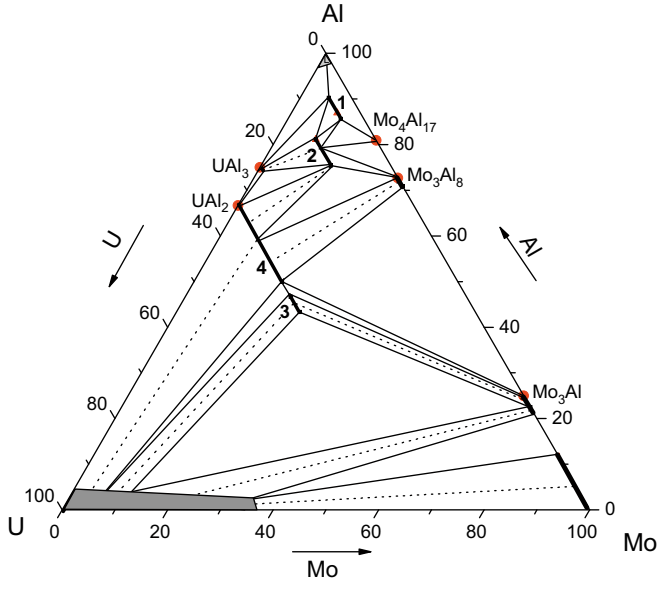

Fig. 1. Phase relations in the ternary U–Mo–Al system, constructed from samples heat-treated at 800 °C and quenched in air: (1) $UMo_{2-x}Al_{20+x}$; (2) $U_6Mo_{4+x}Al_{43-x}$; (3) $UAl_{2-x}Mo_x$ ($MgZn_2$ type); (4) $UAl_{2-x}Mo_x$ ($MgCu_2$ type).

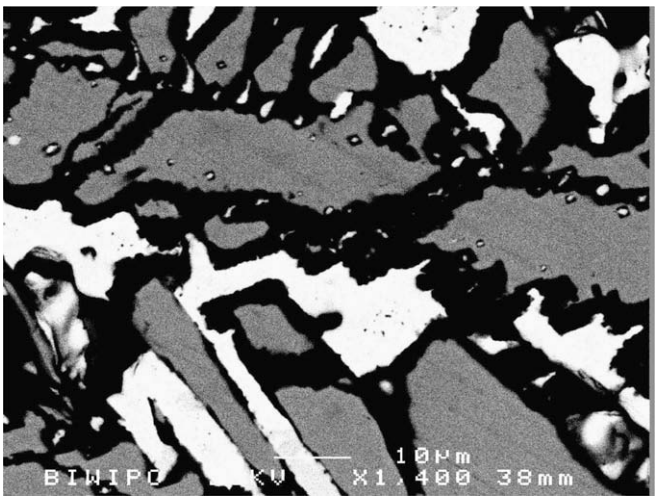

Fig. 2. SEM micrograph of a sample $U_6Mo_4Al_{43}$ annealed at 800 °C: white phase = UAl_3, grey phase = $U_6Mo_5Al_{42}$, black phase = UMo_2Al_{20}.

diffraction and more clearly microprobe analysis revealed that these ternary intermetallics are typically non-stoichiometric, and show significant homogeneity ranges; $U_6Mo_{4+x}Al_{43-x}$ with $0 < x < 3$ and $UMo_{2-x}Al_{20+x}$ with $-0.3 < x < 0.75$ at 800 °C. Similar deviations from the stoichiometric composition were also found in the analogous rare earth-based phases, such as $Ho_6Mo_{4+x}Al_{43-x}$ [10] or $CeMo_{2-x}Al_{20+x}$ [9] and can be thus considered as a predominant feature of these structural types. Quasi-pure samples of the ternary phases may be obtained directly in as-cast samples with initial composition $U_6Mo_7Al_{40}$, and using a slight excess of Al for UMo_2Al_{20} ($UMo_{1.5}Al_{20.5}$), suggesting congruent melting for these compositions.

DTA experiments revealed melting temperatures of 1360 ± 5 °C for $U_6Mo_7Al_{40}$ and 1200 ± 5 °C for UMo_2Al_{20}.

$UMo_{2-x}Al_{20+x}$ is in equilibrium with Al(liquid), UAl_3, $U_6Mo_{4+x}Al_{43-x}$, and Mo_4Al_{17}. The other Al-rich ternary compound $U_6Mo_{4+x}Al_{43-x}$ is in equilibrium with $UMo_{2-x}Al_{20+x}$, UAl_3, $UAl_{2-x}Mo_x$ ($MgCu_2$ type), Mo_3Al_8 and Mo_4Al_{17}.

3.2. Crystal structure refinements of the ternary phases $UMo_{2-x}Al_{20+x}$ and $U_6Mo_{4+x}Al_{43-x}$

In order to determine more accurately the crystallographic site occupations and to obtain further knowledge on the Mo/Al substitution mechanisms, crystal structure refinements of $UMo_{2-x}Al_{20+x}$ and $U_6Mo_{4+x}Al_{43-x}$ have being carried out using single-crystal X-ray diffraction data. Single crystals of the first ternary phases were obtained by the Al flux method, and by annealing for 2 weeks at 950 °C a sample with initial composition of 6:7:40, for the second one. The conditions for crystal data collections are gathered in Table 1, the refined atomic positions are in Table 2 for $UMo_{2-x}Al_{20+x}$ and in Table 3 for $U_6Mo_{4+x}Al_{43-x}$. Selected interatomic distances for $UMo_{2-x}Al_{20+x}$ and $U_6Mo_{4+x}Al_{43-x}$ are listed in Tables 4 and 5, respectively. The refinements, performed with the SHELXS program [18], confirmed that these ternaries $UMo_{2-x}Al_{20+x}$ and $U_6Mo_{4+x}Al_{43-x}$ crystallize with the $CeCr_2Al_{20}$ (cubic, $Fd\bar{3}m$) and the $Ho_6Mo_4Al_{43}$ (hexagonal, $P6_3/mcm$) types, respectively.

For $UMo_{2-x}Al_{20+x}$, refinements of the occupation parameters indicated a mixed occupancy of a *16d* Wyckoff position (of the $Fd\bar{3}m$ space group) by Mo and Al atoms with an electron density corresponding to an occupancy rate of 0.634(5)Mo + 0.366(5)Al. The chemical formula thus deduced from the refinement of this single crystal prepared with a large excess of aluminium, $UMo_{1.27}Al_{20.73}$, is in perfect agreement with the upper limit of the solid solution determined by EDS analysis.

For $U_6Mo_{4+x}Al_{43-x}$, refinements of the occupation parameters indicated a mixed occupancy by Mo and Al atoms of a *8h* Wyckoff position ($P6_3/mmc$ space group) with an electron density corresponding to an occupancy rate of 0.605(3)Mo + 0.395(3)Al. Lower

Table 2
Atomic coordinates and equivalent isotropic displacement parameters (Å^2) for $UMo_{1.27}Al_{20.73}$.

Atom	Wyckoff position	*x*	*y*	*z*	$U_{eq.}$ (Å^2)
U(1)	8a	1/8	1/8	1/8	0.008(1)
Mo(1)[a]	16d	1/2	1/2	1/2	0.006(1)
Al(1)	16c	0	0	0	0.016(1)
Al(2)	48f	0.4880(1)	1/8	1/8	0.014(1)
Al(3)	96g	0.0596(1)	0.0596(1)	0.3240(1)	0.012(1)

U_{eq} is defined as one third of the trace of the orthogonalized U_{ij} tensor.
[a] Occupancy (Mo,0.634(5)–Al,0.366(5)).

Table 3
Atomic coordinates and equivalent isotropic displacement parameters (Å^2) for $U_6Mo_7Al_{40}$.

Atom	Wyckoff position	*x*	*y*	*z*	$U_{eq.}$ (Å^2)
U(1)	12k	0.5313(1)	0	0.0949(1)	0.008(1)
Mo(1)	2b	0	0	0	0.007(1)
Mo(2)	6g	0.7364(1)	0	1/4	0.006(1)
Mo(3)[a]	8h	1/3	2/3	0.1320(1)	0.009(1)
Al(1)	6g	0.1517(1)	0	1/4	0.011(1)
Al(2)[b]	12i	0.4996(1)	0.2498(1)	0	0.015(1)
Al(3)	12j	0.1488(1)	0.5994(1)	1/4	0.010(1)
Al(4)	12k	0.1591(1)	0	0.6138(1)	0.010(1)
Al(5)[c]	12k	0.2565(1)	0	0.0284(1)	0.011(1)
Al(6)	24l	0.1618(1)	0.3964(1)	0.1615(1)	0.011(1)

U_{eq} is defined as one third of the trace of the orthogonalized Uij tensor.
[a] Occupancy (Mo,0.605(3)–Al,0.395(3)).
[b] Occupancy (Al,0.936(3)–Mo,0.064(3)).
[c] Occupancy (Al,0.963(3)–Mo,0.037(3)).

Table 1
Crystal data and structure refinements parameters for $UMo_{2-x}Al_{20+x}$ ($x = 0.73(1)$) and $U_6Mo_{4+x}Al_{43-x}$, ($x = 3.0(1)$).

Empirical formula	$UMo_{1.27}Al_{20.73}$	$U_6Mo_7Al_{40}$
Formula weight (g mol^{-1})	919.1	3179.0
Crystal system, space group	Cubic, $Fd\bar{3}m$ (# 227)	Hexagonal, $P6_3/mcm$ (# 193)
Unit cell dimensions (Å)	$a = 14.495(1)$	$a = 10.955(1)$
		$c = 17.655(1)$
Volume (Å^3)	3045.5(1)	1836.2(1)
Z, Calculated density (g cm^{-3})	8, 4.00	2, 5.75
Absorption coefficient (cm^{-1})	133.6	296
Crystal color and habit	Black, plate like	Black, irregular prism
Crystal size (mm^3)	0.07 × 0.05 × 0.03	0.11 × 0.08 × 0.03
Theta range for data collection (°)	2.43–39.74	3.72–45.00
Limiting indices	$-25 \leqslant h \leqslant 26$	$-21 \leqslant h \leqslant 21$
	$-26 \leqslant k \leqslant 14$	$-18 \leqslant k \leqslant 21$
	$-26 \leqslant l \leqslant 26$	$-34 \leqslant l \leqslant 35$
Reflections collected/unique	15 595/491	65 454/2738
R(int)	0.075	0.117
Absorption correction	Analytical [22]	Semi-empirical from equivalents [23]
Max/min transmission	0.7031/0.4319	0.2838/0.0925
Data/restraints/parameters	491/0/18	2738/0/59
Goodness-of-fit on F^2	1.11	1.01
R indices* [$I > 2(I)$]	$R_1 = 0.0232$, $wR_2 = 0.0573$	$R_1 = 0.0291$, $wR_2 = 0.0417$
Extinction coefficient	0.00016(4)	0.000172(8)
Largest diff. peak and hole (e Å^{-3})	2.64 and −1.53	2.95 and −1.90

* $R(F) = \sum ||F_0| - |F_C||/|F_C|$ (for $F^2 > 2(F^2)$); $wR_2 = \left[\sum w(F_0^2 - F_C^2)/wF_o^4\right]^{1/2}$, where $w^{-1} = [^2(F_0^2) + (Ap)^2 + Bp]$, $p = [\max(F_0^2,0) + 2F_C^2]/3$.

Table 4
Selected interatomic distances (Å) for $UMo_{1.27}Al_{20.73}$.

U(1)–Al(1) × 4	3.138(2)	Mo(2)–Al(2) × 6	2.568(1)
U(1)–Al(3) × 12	3.181(2)	Mo(2)–Al(3) × 6	2.829(2)
Al(1)–Al(3) × 12	3.085(1)	Al(3)–Al(3)	2.683(2)
Al(1)–U(1) × 2	3.138(2)	Al(3)–Al(2)	2.731(2)
		Al(3)–Al(3) × 2	2.737(2)
Al(2)–Mo(2) × 2	2.568(1)	Al(3)–Mo(2)	2.829(2)
Al(2)–Al(3) × 2	2.731(2)	Al(3)–Al(2) 2	2.860(2)
Al(2)–Al(2) × 4	2.808(2)	Al(3)–Al(3) × 2	2.947(2)
Al(2)–Al(3) × 4	2.860(2)	Al(3)–Al(1) × 2	3.085(1)
		Al(3)–U(1)	3.181(2)

Table 5
Selected interatomic distances (Å) for $U_6Mo_7Al_{40}$.

U(1)–Al(6) × 2	3.054(1)	Mo(1)–Al(4) × 6	2.660(2)
U(1)–Al(2) × 2	3.0807(2)	Mo(1)–Al(5) × 6	2.855(1)
U(1)–Al(3) × 2	3.082(1)		
U(1)–Al(5)	3.186(2)	Mo(2)–Al(1) × 2	2.510(1)
U(1)–Al(5)	3.231(2)	Mo(2)–Al(4) × 2	2.665(2)
U(1)–Mo(3) × 2	3.2478(2)	Mo(2)–Al(3) × 2	2.712(2)
U(1)–Al(6) × 2	3.264(1)	Mo(2)–Al(6) × 4	2.725(1)
U(1)–Al(2) × 2	3.3725(2)		
U(1)–Al(4)	3.408(2)	Mo(3)–Al(6) × 3	2.647(1)
U(1)–U(1)	3.424(1)	Mo(3)–Al(3) × 3	2.736(1)
		Mo(3)–Al(2) × 3	2.820(1)
Al(1)–Mo(2) × 2	2.510(1)	Mo(3)–U(1) × 3	3.248(1)
Al(1)–Al(6) × 4	2.832(2)		
Al(1)–Al(1) × 2	2.878(3)	Al(2)–Al(2) × 2	2.746(2)
Al(1)–Al(4) × 4	2.949(2)	Al(2)–Al(5) × 2	2.747(1)
		Al(2)–Mo(3) × 2	2.820(1)
Al(3)–Mo(2)	2.712(2)	Al(2)–U(1) × 2	3.081(1)
Al(3)–Mo(3) × 2	2.736(1)	Al(2)–U(1) × 2	3.372(1)
Al(3)–Al(6) × 2	2.778(2)		
Al(3)–Al(6) × 2	2.780(2)	Al(4)–Mo(1)	2.660(2)
Al(3)–Al(3)	2.823(2)	Al(4)–Mo(2)	2.665(2)
Al(3)–U(1) × 2	3.082(1)	Al(4)–Al(6) × 2	2.719(2)
		Al(4)–Al(5)	2.729(2)
Al(5)–Al(4)	2.729(2)	Al(4)–Al(5) × 2	2.883(2)
Al(5)–Al(2)	2.747(1)	Al(4)–Al(1) × 2	2.949(2)
Al(5)–Mo(1)	2.855 (1)	Al(4)–U(1)	3.408(2)
Al(5)–Al(6) × 2	2.881(2)		
Al(5)–Al(4) × 2	2.883(2)	Al(6)–Mo(3)	2.647(1)
Al(5)–Al(5) × 2	2.985(2)	Al(6)–Al(4)	2.719(1)
Al(5)–U(1)	3.186(2)	Al(6)–Mo(2)	2.725(1)
Al(5)–U(1)	3.231(2)	Al(6)–Al(3)	2.778(2)
		Al(6)–Al(3)	2.780(2)
		Al(6)–Al(1)	2.832(2)
		Al(6)–Al(5)	2.881(2)
		Al(6)–U(1)	3.054(1)
		Al(6)–U(1)	3.264(1)

substitution rates (6.4% and 3.7%) of the Al(2) and Al(5) sites (in 12i and 12k) by Mo are also indicated from the refinements. The chemical formula deduced from the structural refinement, $U_6Mo_7Al_{40}$, is also in perfect agreement with the starting composition of the sample and EDS analysis. In the prototype compound $Ho_6Mo_4Al_{43}$, as well as in the titanium-based ternaries such as $Dy_6Ti_4Al_{43}$, [19] the *8h* crystallographic site is occupied essentially by Al atoms, whereas in $U_6Mo_7Al_{40}$, a main occupation by Mo leads to a more stable composition.

3.3. The U–Mo–Al phase diagram of quenched samples heat-treated at 400 °C

As mentioned in the introduction, it is of large interest to perfectly know the room temperature phase relations of this system from samples heat-treated at 400 °C which, in the industrial process of fabrication of the U–Mo/Al fuel plates, corresponds to the temperature of the hot rolling of the plates.

The U–Mo–Al phase diagram obtained after annealing the arc-melted samples at 400 °C during 2 months is shown in Fig. 3.

3.3.1. Binary and pseudo-binary phases

UAl_4, which forms peritectally at 731 °C [12] has been confirmed to be a stoichiometric compound, as previously reported [11] and does not dissolves any significant amount of molybdenum. Two more phases: $MoAl_5$ and $MoAl_{12}$ are reported to be stable in the Mo–Al system [12]. The binary alloy U_2Mo (often called γ′ phase) could not be clearly observed in our experiments (Al containing alloys), but the cubic γ form of the U–Mo alloys was found to be stable after 2 months of annealing at 400 °C , for Mo contents higher than ≈10 at.% (4.1 wt%). This behaviour is essential for a qualification of U–Mo alloys as nuclear fuels, but is not in agreement with the assessed binary equilibrium phase diagram [12] and previously published data on the U–Mo–Al system [8]. As already mentioned, a metastable state of the cubic γ form at room temperature is then indicated in literature for this concentration domain, but long time annealings at 400 °C indicate a high stability rather than a metastability. It should be also mentioned that no signs of phase transition could be evidenced by DSC experiments on γ-stabilized U–Mo powders [15], giving more argument for some revision of the binary Mo–U equilibrium phase diagram (see comments in [12]).

3.3.2. The ternary phases

As shown in Fig. 3, the ternary phases present in the system are the same as at 800 °C, with, however, apparently larger homogeneity domains than observed at 800 °C, which is not coherent. For instance, elementary EDS analysis indicate that $UAl_{2-x}Mo_x$ with the $MgZn_2$ type is formed within the limits $0.70 < x < 0.85$ at $T = 400$ °C (compared to $0.6 < x < 0.7$ at $T = 800$ °C). These values are similar to those measured in as-cast samples, indicating that re-ordering of atoms in the mixed crystallographic sites from the as-cast state is not achieved at 400 °C after 2 months of annealing.

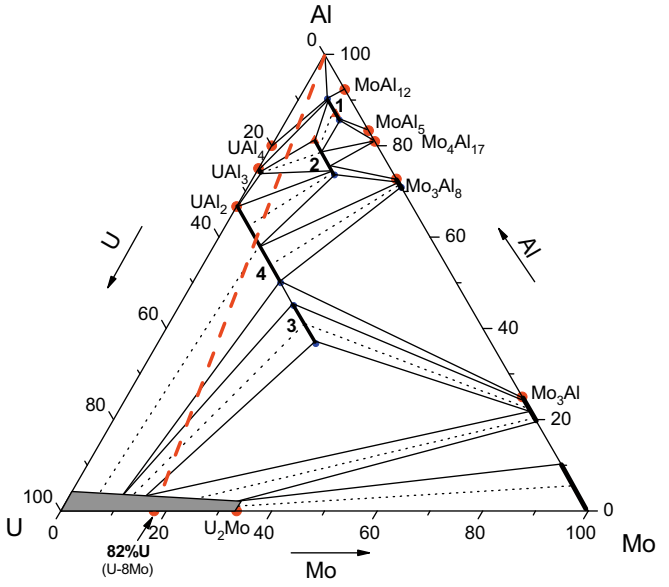

Fig. 3. Phase relations in the ternary U–Mo–Al system, constructed from samples heat-treated at 400 °C and quenched in air: (1) $UMo_{2-x}Al_{20+x}$; (2) $U_6Mo_{4+x}Al_{43-x}$; (3) $UAl_{2-x}Mo_x$ ($MgZn_2$ type); (4) $UAl_{2-x}Mo_x$ ($MgCu_2$ type). Thick dashed line = interaction path U–8Mo/Al.

3.3.3. Phase relations and the U–Mo(fuel)/Al(matrix) interaction

The thick dotted line on Fig. 3 represents the interaction line between the U–8 wt%Mo fuel (in γ form) with the Al matrix. It crosses successively the tie-lines UAl_4–$UMo_{2-x}Al_{20+x}$, UAl_3–$UMo_{2-x}Al_{20+x}$, UAl_3–$U_6Mo_{4+x}Al_{43-x}$ and $UAl_{2-x}Mo_x$–$U_6Mo_{4+x}Al_{43-x}$.

The nature of the successive interaction layers (thermal activated formation), observed both in fuel plates and in diffusion couple studies [20,21] can be thus deduced in according to this phase diagram study. Their compositions alternate the above mentioned two-phase equilibria and the three-phase fields which correspond to the successive interaction zones:

$$\text{First interaction zone} = Al + UAl_4 + UMo_{2-x}Al_{20+x}, \quad (1)$$

$$\text{Second interaction zone} = UAl_4 + UAl_3 + UMo_{2-x}Al_{20+x}, \quad (2)$$

$$\text{Third interaction zone} = UAl_3 + UMo_{2-x}Al_{20+x} + U_6Mo_{4+x}Al_{43-x}. \quad (3)$$

Ultimately, in the presence of a sufficient amount of Al powder, after long time interaction or/and increase of temperature, the γ-UMo fuel particles could be totally consumed to form the UAl_{2-x}-Mo_x cubic phase, which is itself expected to be stable thermally and under irradiation.

4. Conclusion

Phase relations in the U–Mo–Al ternary system established from quenched samples heat-treated at 800 °C and 400 °C have been constructed. Our results indicate that the two previously reported ternary phases $U_6Mo_{4+x}Al_{43-x}$ and $UMo_{2-x}Al_{20+x}$ show significant homogeneity ranges resulting from mixed (Mo,Al) crystallographic sites occupations. The solubility of Mo in UAl_3 and in UAl_4 is very low or negligible, whereas the solubility of Mo amounts up to 25% of Al in UAl_2 with retaining the cubic $MgCu_2$-type structure, and undergoing to the hexagonal $MgZn_2$-type $UAl_{2-x}Mo_x$ pseudo-ternary Laves phase for higher Mo contents. The ternary phase diagram informs about the interactions between the γU–Mo fuel particles with the Al powder matrix, yielding to the successive formation of $UMo_{2-x}Al_{20+x}$, UAl_4, UAl_3, and $U_6Mo_{4+x}Al_{43-x}$. These phases appear in interaction layers from the outer part to the inner core of the U–Mo particles, with compositions determined by the equilibrium states in the ternary fields from the Al-rich to -poor regions of the phase diagram.

References

[1] B.W. Howlett, A.J. Eycott, I.K. Kang, D.R.F. West, J. Nucl. Mater. 9 (1963) 143.
[2] G.L. Hofman, M.R. Finlay, Y.S. Kim, in: International Meeting on Reduced Enrichment for Research and Test Reactors (RERTR), Vienna, Austria, 7–12 November 2004.
[3] P. Lemoine, J.L. Snelgrove, N. Arkhangelsky, L. Alvarez, in: Eighth International Topical Meeting on Research Reactor Fuel Management (RRFM), München, Germany, 21–24 March, 2004.
[4] A. Leenaers, S. Van den Berghe, E. Koonen, C. Jarousse, F. Huet, M. Trotabas, M. Boyard, S. Guillot, L. Sannen, M. Verwerft, J. Nucl. Mater. 335 (2004) 39.
[5] J.S. Lee, C.H. Lee, K.H. Kim, V. Em, J. Nucl. Mater. 306 (2002) 147.
[6] M.I. Mirandou, S.N. Balart, M. Ortiz, M.S. Granovsky, J. Nucl. Mater. 323 (2003) 29.
[7] K.H. Kim, D.B. Lee, C.K. Kim, G.L. Hofman, K.W. Paik, Nucl. Eng. Des. 178 (1997) 111.
[8] G. Petzow, J. Rexer, Z. Metallkd. 62 (1971) 34.
[9] S. Niemann, W. Jeitschko, J. Solid State Chem. 114 (1995) 337.
[10] S. Niemann, W. Jeitschko, Z. Metallkd. 85 (1994) 345.
[11] O. Tougait, H. Noël, Intermetallics 12 (2004) 219.
[12] T.B. Massalski, Binary Alloy Phase Diagrams, second Ed., ASM International, Materials Park, OH, 1990.
[13] Pauling File, CD ROM, in: P. Villars (Ed.), Distributed by ASM International, 2006.
[14] J.C. Schuster, H. Ipser, Metall. Trans. 22A (1991) 1729.
[15] K.H. Kim, D.B. Lee, C.K. Kim, G.E. Hofman, K.W. Paik, J. Nucl. Mater. 245 (1997) 79.
[16] S.C. Parida, S. Dash, Z. Singh, R. Prasad, V. Venugopal, J. Phys. Chem. Solid. 62 (2001) 585.
[17] D.D. Keiser Jr., C.R. Clark, M.K. Meyer, Scr. Mater. 51 (2004) 893.
[18] G.M. Sheldrick, SHELX-97, Program for Crystal Structure Refinement, University of Göttingen, Germany, 1997.
[19] S. Niemann, W. Jeitschko, J. Solid State Chem. 116 (1995) 131.
[20] H. Palancher, P. Martin, V. Nassif, R. Tucoulou, O. Proux, J.L. Hazemann, O. Tougait, E. Lahéra, F. Mazaudier, C. Valot, S. Dubois, J. Appl. Crystallogr. 40 (2007) 1064.
[21] F. Mazaudier, C. Proye, F. Hodaj, J. Nucl. Mater. 377 (2008) 476.
[22] J. de Meulenaar, H. Tompa, Acta Crystallogr. Sect. A 19 (1965) 1014.
[23] R.H. Blessing, Acta Crystallogr. Sect. A. 51 (1995) 33.